LAWRENCE
LIVERMORE
NATIONAL
LABORATORY

LLNL-CONF-657947

Target material collection for High Energy Imaging Diagnostic

M. F. Ahmed, J. M. Mcnaney, R. M. Vignes, C. A. Smith, N. Masters, C. Bailey, R. B. Petre

July 31, 2014

SPIE Optics + Photonics 2014
San Diego, CA, United States
August 17, 2014 through August 20, 2014

Disclaimer

Target material collection for High Energy Imaging Diagnostic

Maryum F. Ahmed, James M. Mcnaney, Ryan M. Vignes, Cal A. Smith, Nathan Masters

Chris Bailey, Robert B. Petre

Lawrence Livermore National Laboratory, 7000 East Avenue, Livermore, CA 94550

ABSTRACT

The National Ignition Facility (NIF) at Lawrence Livermore National Laboratory uses the world's largest and most energetic laser system to explore Inertial Confinement Fusion (ICF) and High-Energy-Density (HED) physics, with the potential of creating pressure and density conditions normally found in the cores of stars or large planets. During NIF experiments, the laser energy is directed to the target, driving the desired physics conditions, and the breakup of the target. During this breakup there is the potential to generate debris fields with both vaporized and solid target material, traveling at extremely high velocities (~10 km/s). For future shots, it is desirable to minimize distribution of the certain target materials within NIF. The High Energy Imaging Diagnostic (HEIDI), which comes within 8 cm of the target, will be modified to minimize the distribution of the ejected material. An external cone will be added to HEIDI which will block a larger angle than the existing hardware. Internal shielding will be added to isolate target material within the front portion of the diagnostic. A thin aluminum bumper will slow low-density vaporized material and contribute to the breakup of high velocity particles, while a thicker wall will block solid chunks. After the shot, an external cover will be installed, to contain any stray material that might be disturbed by regular operations. The target material will be retrieved from the various shielding mechanisms and assayed.

Keywords: High Energy Imaging Diagnostic, HEIDI, NIF, capture, high-energy-density, HED

1. INTRODUCTION

The National Ignition Facility (NIF), located at Lawrence Livermore National Laboratory (LLNL) is the highest energy laser ever constructed[1]. The High Energy Imaging Diagnostic (HEIDI) is an x-ray imaging platform used on NIF in support of High Energy Density (HED) experiments. A portion of the target material used in experiments is deposited on HEIDI, due to HEIDI's proximity to the target assembly at the time of the NIF shot. HEIDI will be modified to control the distribution of ejected target material in NIF and to limit the exposure of personal to target material. After the completion of the experiment, the material will be assayed and inventoried.

1.1 High Energy Density Campaign

Along with the mission to achieve fusion ignition, NIF was created to support HED experiments in support of the nation's Stockpile Stewardship program. The NIF lasers can be used to produce very high pressures, high radiation temperatures and highly convergent implosions. Large amounts of energy, e.g. up to 1.8 MJ on NIF, can be coupled into small, well-defined volumes to achieve high energy densities over a wide range of timescales (picoseconds to hundreds of nanoseconds) [2]. NIF enables quantitative experiments to validate the codes and models of the nuclear phase of weapon operations[3].

1.2 ALARA Principles

ALARA, an acronym for "as low as reasonably achievable" is a process incorporated into LLNL's environmental program, which manages operations involving the use of radioactive materials. The goal of the process is to protect the health and safety of LLNL employees, contractors, the general public and the environment[4].

To adhere to the principles of ALARA, the HEIDI diagnostic will be modified to minimize contamination of the HEIDI assembly and control distribution of target material within the NIF facility. The updated diagnostic is referred to as HEIDI-C.

2. HEIDI BACKGROUND

HEIDI measures 2D time integrated point-projection radiographs illuminated by high-energy x-ray backlighters. A multi-layered shielded enclosure houses a passive x-ray detector (image plate[6]). The enclosure shielding consists of a full-length aluminum core and tungsten outer layer to mitigate fluorescence and reduce high-energy x-rays background on the data. The nose cone includes a tungsten aperture to further reduce the x-ray background on the image. A filter holder is located approximately midway between the collimator and the image plate, allowing for the use of various filter materials. A filter-stack spectrometer is located behind the x-ray detector to measure the backlighter spectrum. The overall length of the HEIDI diagnostic is approximately 73 cm.

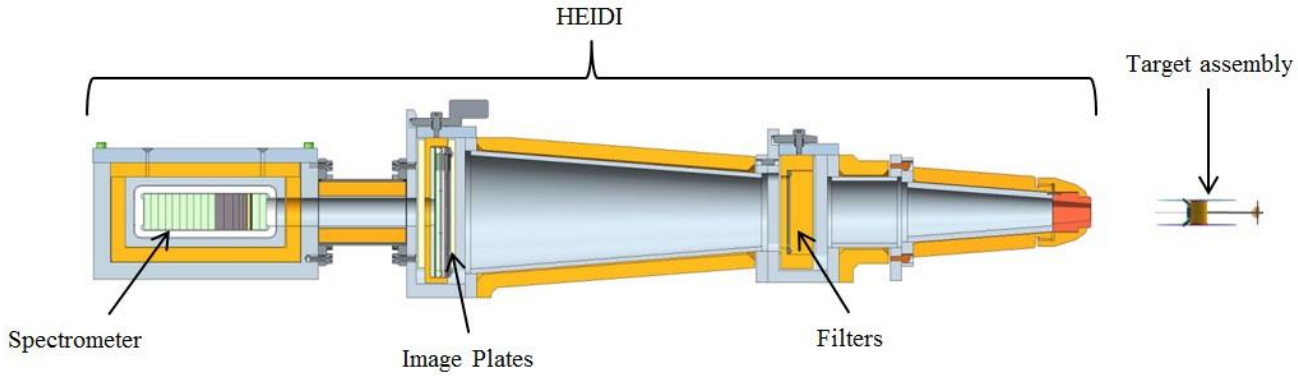

Figure 1. The HEIDI assembly includes an aperture, filters, image plates and spectrometer. The experimental package on the target assembly is oriented towards the HEIDI nose cone.

HEIDI is positioned and aligned in the NIF target chamber using one of the Diagnostic Instrument Manipulators (DIM). The DIMs are two-stage, telescoping systems used with many of the NIF diagnostics. The DIMs have been upgraded to reduce worker exposure to radiological contamination, in adherence to the ALARA principles[5]. The upgraded HEIDI-C design will incorporate physical and operational changes to minimize exposure of DIM workers.

2.1 Target assembly

For the HED experimental campaign for which HEIDI-C has been developed, the material of interest (MOI) (i.e., the material studied by the experiment and the material that will be assayed and inventoried), as part of what will be referred to as the experimental package, is mounted to the side of a hohlraum (with walls consisting of 2 μm of gold and 110 μm of plastic. The experimental package is oriented towards HEIDI, as shown in Figure 1. 1 mm thick Gold shields designed to reduce the x-ray background from the hohlraum and plume emissions are mounted above and below the experimental package. Figure 2 shows the layout of the target assembly components.

NIF laser beams enter the hohlraum from above and below, as shown in Figure 3. The laser light is converted to x-rays, creating high energy density conditions. This energy drives the material of interest towards the HEIDI diagnostic. The entire target assembly creates shrapnel which impacts the HEIDI assembly, both externally and internally. By the time that the target assembly explosion becomes important, the experimental data from the driven experimental package illuminated by the backlighter source has already been collected.

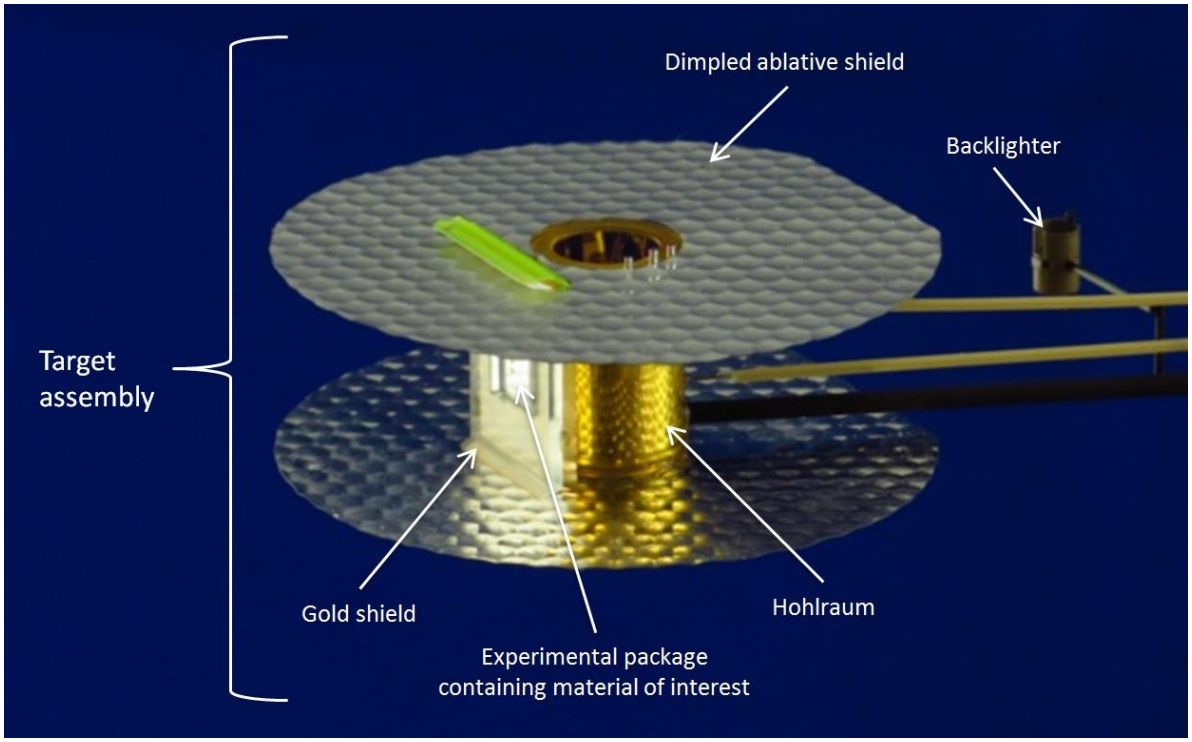

Figure 2. Target assembly major components include the hohlraum, gold shields, experimental package containing the material of interest, and dimpled ablative shields.

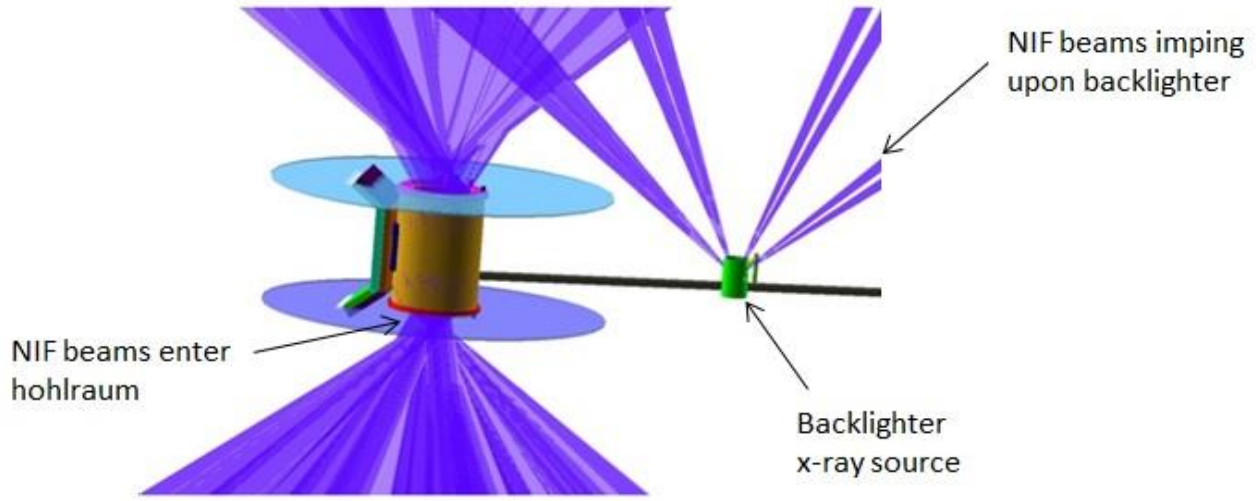

Figure 3. NIF beams imping upon target assembly.

3. RESULTS FROM PREVIOUS HEIDI EXPERIMENTS

Post-shot inspections of HEIDI from previous shots identified debris from the exploding target assembly deposited on the HEIDI nose cone and within the HEIDI line of sight (interior). Figure 4(a) shows the HEIDI aperture and cap, located at the front end of the diagnostic, before a NIF laser shot. Figure 4(b) shows the same parts after the shot.

Materials in filter pack, located approximately midway between the aperture and the image plate pack (~52.5 cm from TCC, see Figure 1) also show damage after shot. Figure 5(a) shows an assembled filter pack with layers of aluminum

polyimide filters. Figure 5(b) shows the same filter pack after the shot. The filters exhibit burns and debris punctures from shrapnel that has traveled down the line of sight of the diagnostic.

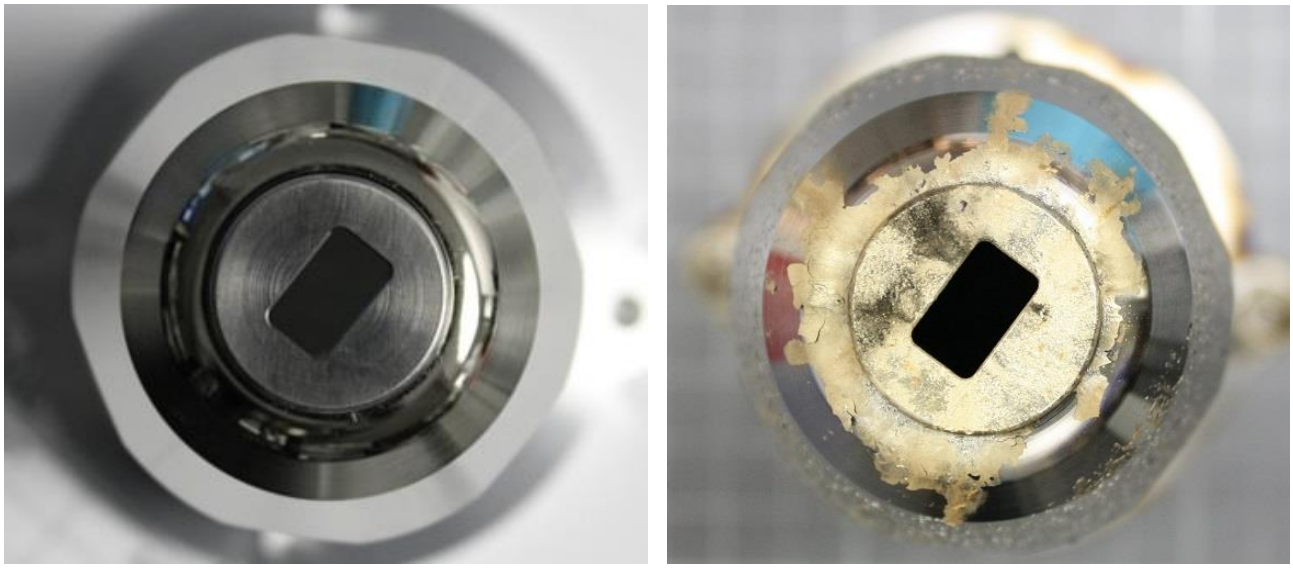

(a) (b)

Figure 4. HEIDI nose cone assembly (a) before a NIF shot and (b) after a NIF shot, showing gold deposition after shot.

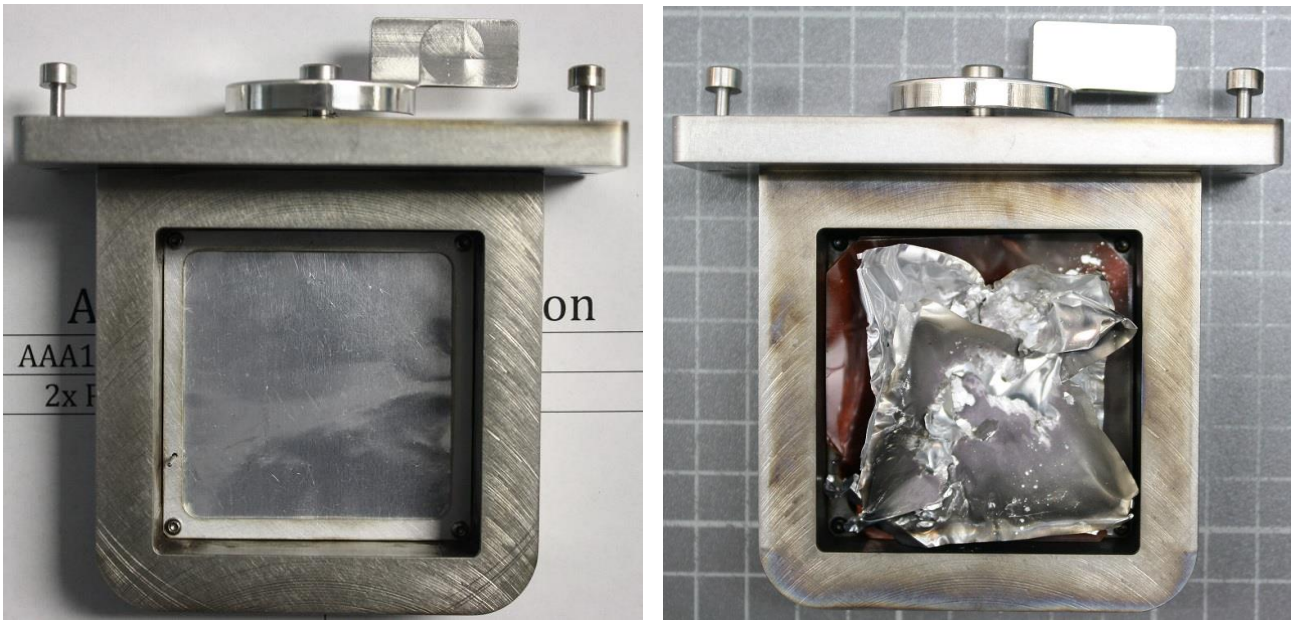

(a) (b)

Figure 5. The HEIDI filter pack (a) before the NIF shot and (b) after the NIF shot, showing burn and debris damage.

4. HEIDI-C UPGRADES

HEIDI-C will incorporate physical and operational changes to adhere to ALARA principles. The upgraded design will minimize contamination in locations where personnel frequently work or where there is risk for spread of contamination. The assembly's nose cone will be modified to isolate the material of interest. This portion will be sent for material assay, a destructive process which will prevent reuse of nose cone components. The modifications will minimize contamination in the aft portion of the diagnostic, which will be reused.

Modifications include an external shield to prevent debris from contacting the external surfaces of the assembly, aft of the nose cone assembly. The attachment of the nose cone assembly will be modified to facilitate removal operations. Internal shielding will be included in the nose cone to prevent debris from traveling down the line of sight to the internal components aft of the nose cone assembly.

After the shot, disturbances of the deposited materials on the contaminated surfaces will be controlled with the installation of a nylon cover.

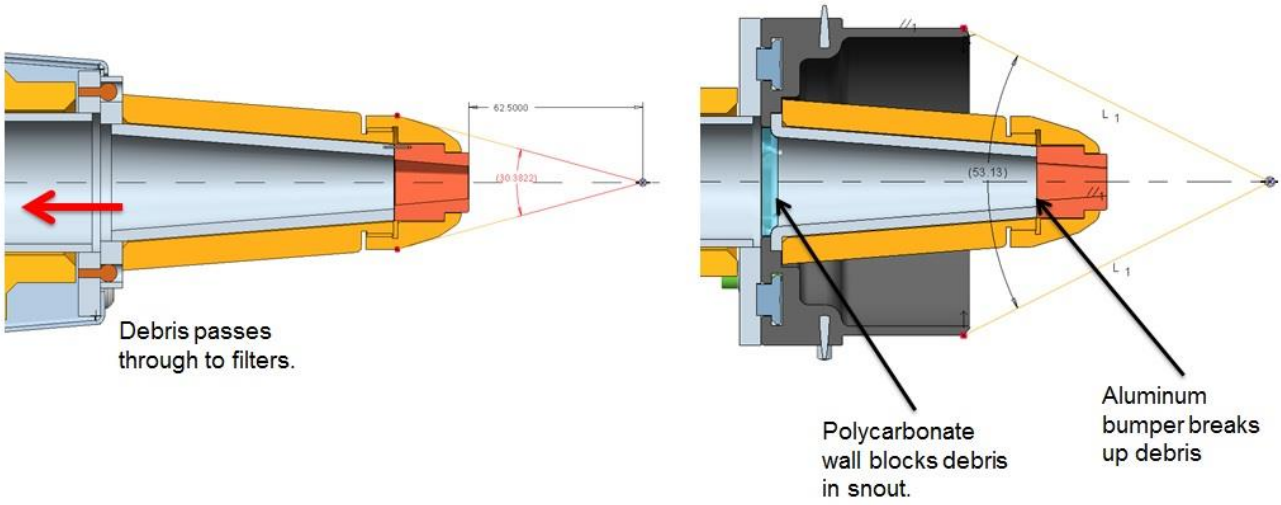

(a) (b)

Figure 6 (a) Current HEIDI nose cone design shields a 30° angle and allows debris to pass through to the filter assembly. (b) The upgraded HEIDI-C will shield a 53° angle and block target debris from traveling aft of the nose cone assembly.

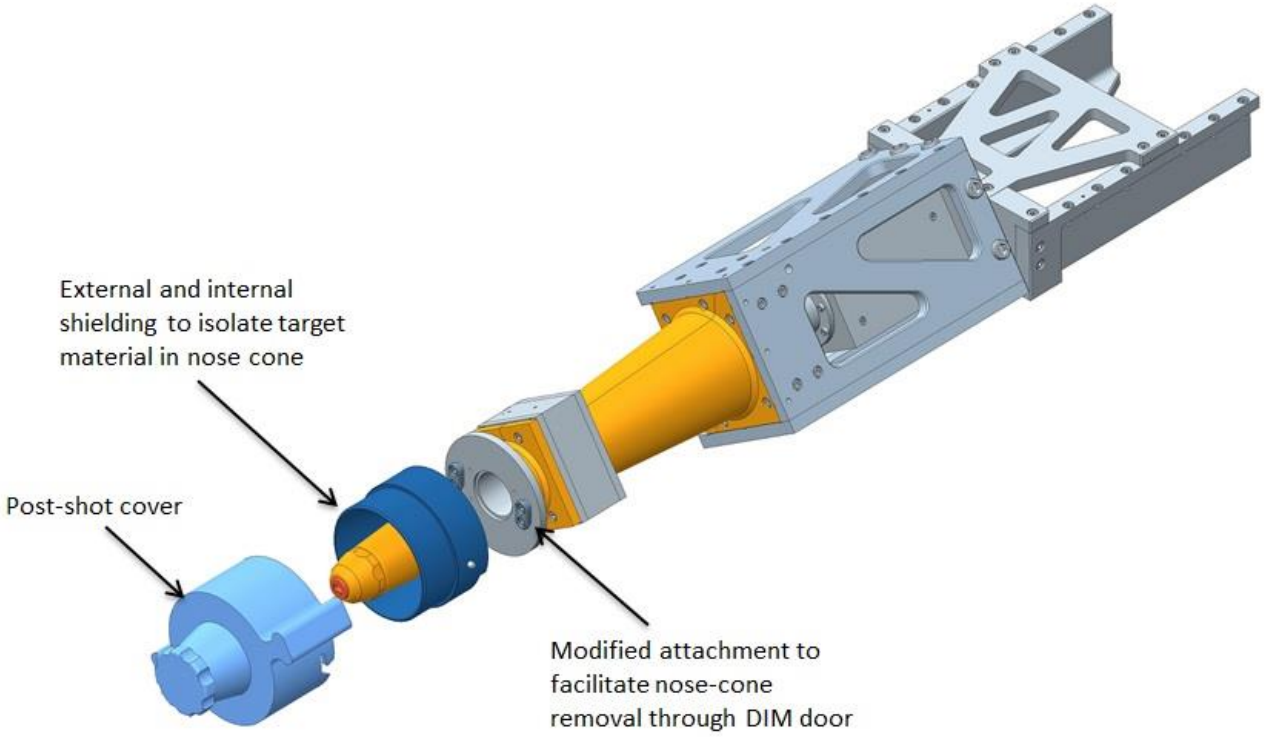

Figure 7. HEIDI-C will incorporate physical and operational changes to adhere to ALARA principles.

4.1 Analysis of external nose cone components

The aperture, located at the tip of the nose cone assembly, and the external shield are loaded by both debris wind and shrapnel. Simulations were performed using the Lawrence Livermore National Laboratory multiphysics hydrocode ALE3D[7] to evaluate damage, penetration and secondary projectile generation. Advantage was taken of the symmetry present in HEIDI to create a refined localized model to represent a quarter symmetric section of the components, as shown in Figure 8.

Separate hydrocode simulations of the hohlraum-target breakup identified potential characteristics of vaporized and non-vaporized (molten) material that is ejected from the target assembly. The analyses of the external components are based on the results of the target assembly breakup analysis. The non-vaporized material was applied to the shrapnel analysis of the external system components. The vaporized material was applied to the wind loading analysis.

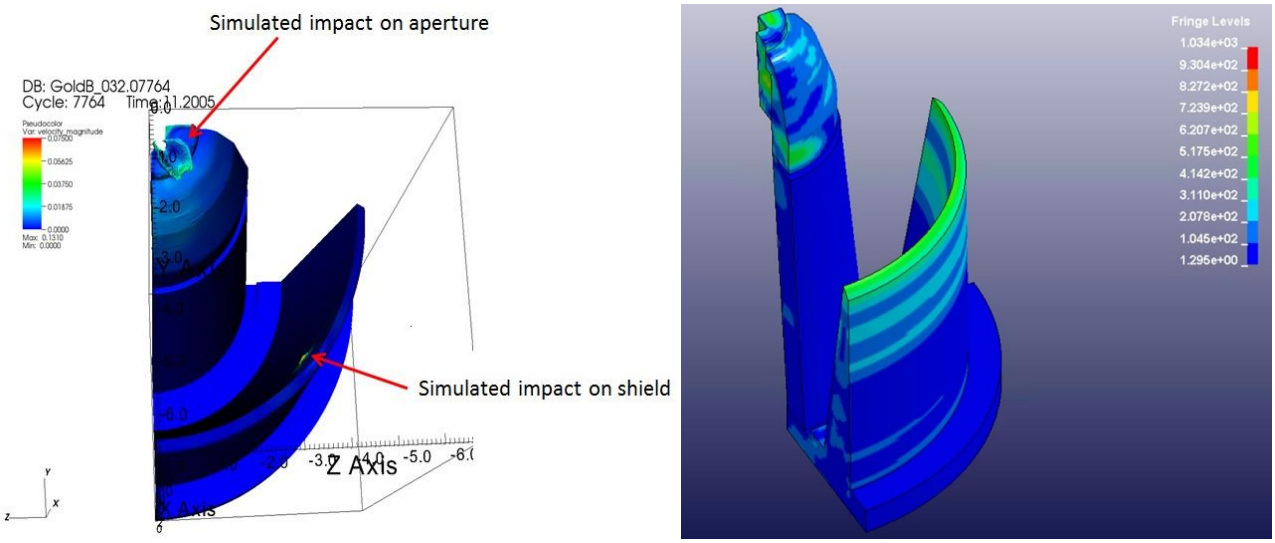

(a) (b)

Figure 8. (a) Velocity plot used to evaluate impact of shrapnel. (b) Stress results from debris wind simulation.

The shrapnel analysis conservatively uses the entire mass of non-vaporized material as a single projectile, though empirically, it is observed that there is target breakup. The shrapnel impact simulation was performed using a 72 mg sphere of molten gold traveling at 2050 m/s. Two impact locations were chosen to represent the worst case that could cause penetration or generate secondary debris: the edge of the tungsten alloy aperture and the edge of the stainless steel shield; the latter considered the worst case because it is the thinnest section. Figure 8 shows the location of the two simulated impactors. The impact on the shield side wall produced localized yield and denting, but no secondary debris was identified. The risk of penetration by shrapnel is low. The impact to the tungsten alloy aperture formed a large crater and may cause disassembly complications, but did not generate secondary debris that would put the NIF optics at risk.

The NIF debris wind is a representation of the expansion of the vaporized mass of the NIF target. It is assumed to be a spherically expanding shell of finite thickness traveling at approximately 100,000 m/s, with a loading duration on the exposed surface of approximately 3 micro-seconds. The expanding shell is anisotropic, with the vertical loading being approximately 2 times higher than the lateral loading, primarily driven by the direction and geometry of the Hohlraum. . Peak pressures in the lateral direction of approximately 3.7 GPa are typical for distances of 62.5 mm from the target The simulated debris wind load, scaled to correspond to the target mass, laser energy, and approximate standoffs of the effected surfaces of the HEIDI diagnostic was applied to surfaces with a line of sight to the blast center. The blast produces localized yielding but does not produce gross deformation of the components.

4.2 Analysis of internal shielding components

The analysis of the internal shielding components used damage results from previous experiments, rather than the target breakup simulation used in the analysis of the external components. This allowed for a less conservative and more experimentally representative estimate of the debris mass.

It should be noted that the recommended barrier thickness found in this analysis must be balanced with the physics requirements, which may limit the acceptable attenuation of the x-ray signal. The maximum thickness must be determined for each experiment based on the physics requirements, and in some cases, may be lower than the recommended barrier thickness. This is the case for the wall tests that will be described in section 5.

4.2.1 Estimating the Debris Threat

To gather statistics on the debris threat, the post-shot front apertures were retrieved and the craters left in the surface from the debris were measured. Figure 9 contains a post-shot image of one of the apertures. From this nose cap, the crater pit depths and diameters were measured. Together, the pit depth and diameter allowed for unique characterization of the craters. Figure 10 contains the pit depth and pit diameter measurements from the three HEIDI shots.

Although there is no evidence that debris similar to that collected by the HEIDI nose cap passed through the snout aperture, only slight changes in alignment or target fracturing and disassembly would be needed to direct debris into HEIDI—potential damaging the filter wall and contaminating the resusable rear portion of the diagnostic. To prevent this, the wall must be thick enough to arrest the most damaging of this debris. From Figure 10, this would be the debris that left the deepest pit (top-most red triangle), or the debris that created the largest diameter crater (right-most black star). In practice there must be a balance between component reuse, ALARA, and allowable filtration from an imaging standpoint.

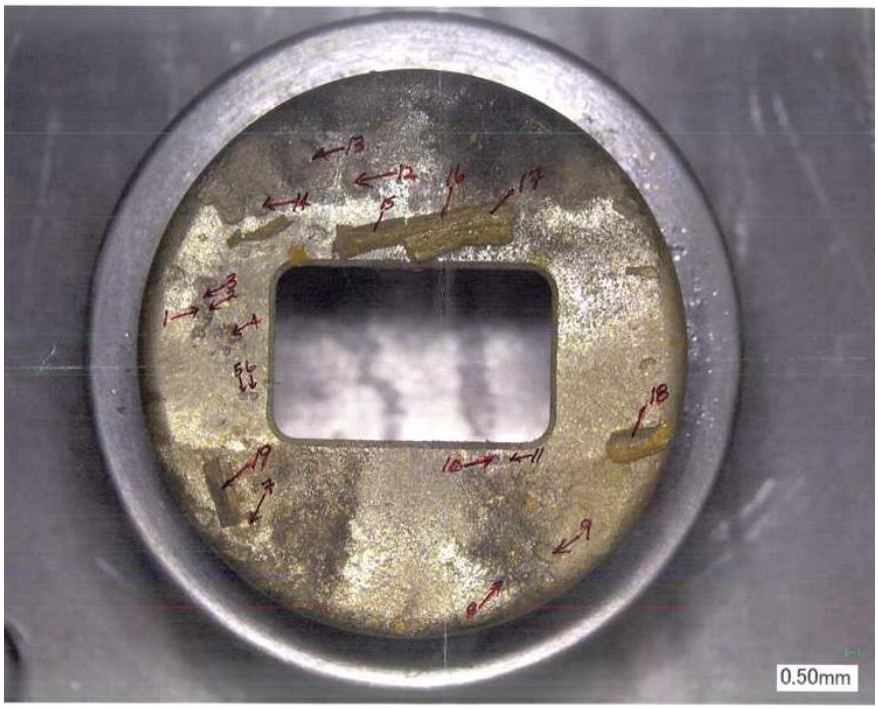

Figure 9. Post shot HEIDI nose cap used to estimate debris field threat.

To determine the size and velocity of the debris that created this damage, simulations were run where the initial velocity and diameter of a gold sphere were prescribed. The gold particle then impacted a tungsten alloy wall model of the HEIDI aperture. The resulting pit depth and diameter were measured and compared to the experimental data shown in Figure 10. In this manner, the debris threat for HEIDI could be mapped out. This resulted in a debris field with gold particles

traveling between 0.5 and 8 km/s and with diameters between 0.05 mm and 0.5mm. The particle size was skewed towards the smaller diameters.

The debris which resulted in the deepest pit (top red triangle) required a gold particle to be traveling at 7 km/s and have a diameter of 0.125 mm (0.02 mg). To create the largest diameter pit (right black star) the gold particle had to travel around 850 m/s with a diameter of 0.5 mm (1.3 mg).

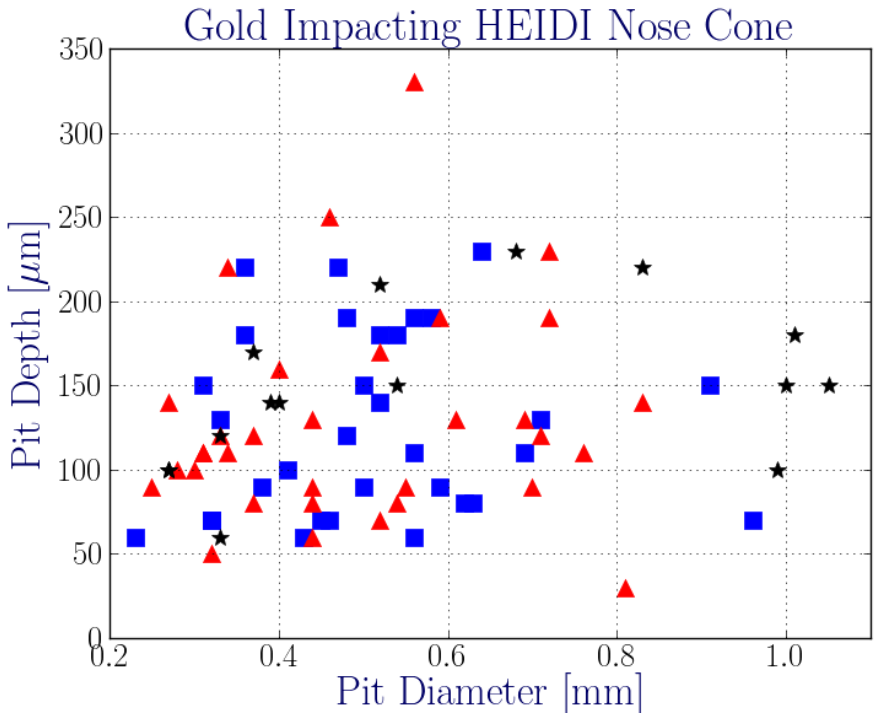

Figure 10. Pit depth and pit diameters from three HEIDI shots. Color coding indicates craters from the same nose cap.

4.2.2 Influence of thin front bumper

For the expected distribution of velocities, the simulations predict that the bumper is largely ineffective until the diameter of the debris approaches a thickness similar to the bumper thickness. When this occurs, the bumper is able to produce particle break-up as it travels toward the wall barrier. Figure 11 contains an example of the debris break-up due to the bumper.

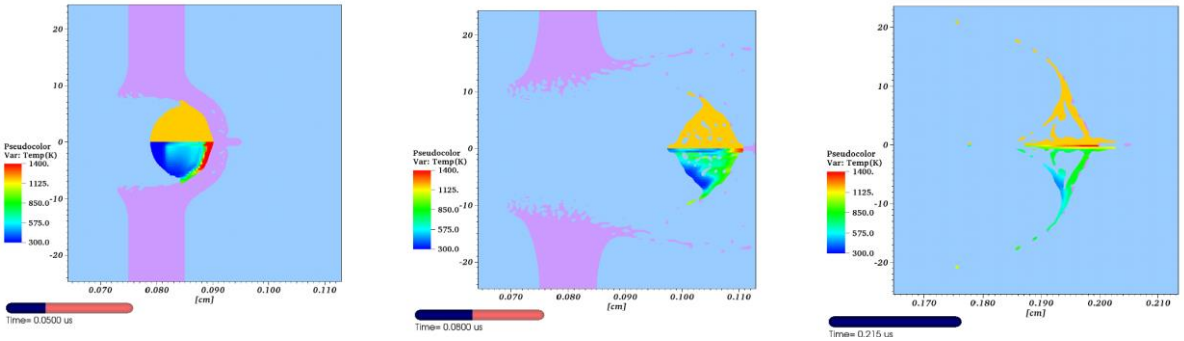

Figure 11. Debris impacting front bumper and breaking-up as it travels towards the wall barrier. Due to the break-up, this debris will be less damaging to the wall barrier.

4.2.3 Wall Barrier Thickness Required to Arrest Debris

With the debris threat determined, it was possible to estimate the wall thickness required to prevent contamination. Two debris threat cases were examined: the one which resulted in the largest pit depth and the one which resulted in the largest pit diameter. These two cases bounded the damage created by the other particles. If the wall can prevent contamination against these two cases, it will be able to prevent contamination from the other debris.

To determine the necessary wall thickness, a 2.4 mm wall and 100 µm bumper were modeled. For computational purposes, the gap between the bumper and wall was only 4.6 mm while in experiments it will be 100 mm. Due to the large gap distance between walls, if debris is broken-up while passing through the bumper, it will disperse before impacting the wall barrier, resulting in less damage to the wall barrier. Using this model, several axisymmetric simulations were run where the particle size and velocity were held constant and the rear wall barrier thickness was varied. The wall thickness was increased until the wall halted the debris. Figure 12 shows the residual particle momentum as wall thickness increases for the two debris threat bounding cases. To arrest both debris threats, the wall barrier must be at least 5.5mm thick.

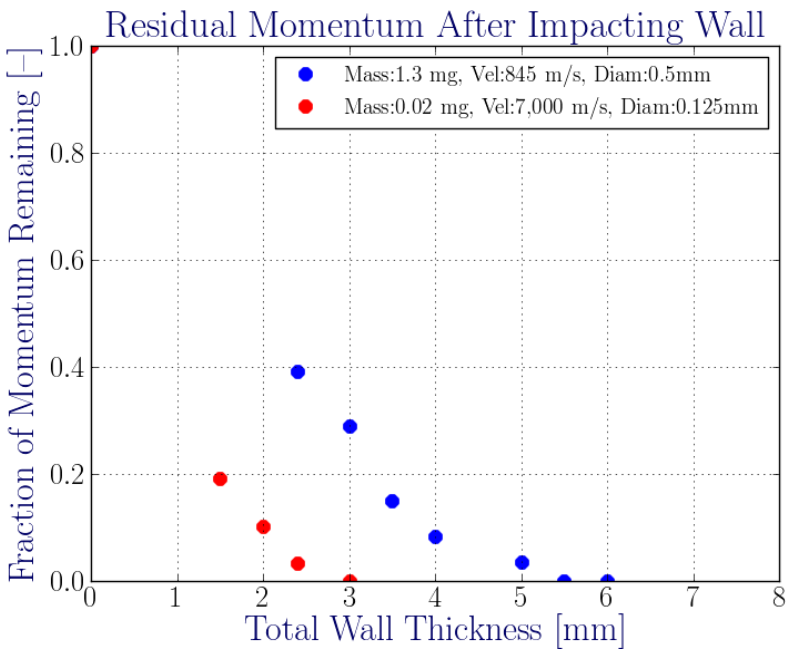

Figure 12. Residual debris momentum after impacting wall barrier. Non-zero momentum indicates the debris penetrated the wall and contaminated the rear portion of HEIDI.

Figure 13 shows a simulation of the wall barrier after the debris has been arrested. The simulation shows that a 5.5 mm thick wall barrier will arrest the most damaging particle debris, however, the wall barrier will be destroyed by the time slower moving debris arrives at the wall. With the wall already destroyed and thoroughly fractured, the slower moving debris will be able to pass through the barrier unimpeded. Based on this simulated result, the wall barrier must be thicker than the minimum 5.5 mm required to arrest the most damaging debris to ensure this does not occur.

From Figure 10, the most damaging debris scenario (debris that produces deep craters), is present in all three experimental results. To date, the largest debris has impacted the nose cone only, and has not entered the nose cone aperture. With this type of debris produced in each experiment, it would appear to be a function of the target assembly geometry, and not due to the statistical nature of fracture mechanics. Since this debris is readily reproducible, there is a non-zero probability that it could enter HEIDI, impacting the wall barrier, and produce damage similar to that shown in the simulation. In such a scenario, the image plates are protected inside the image plate pack, behind additional layers of filter material, which minimizes the risk of image plate exposure to radioactive material. Operational controls minimize the risk of spreading contamination in the facility.

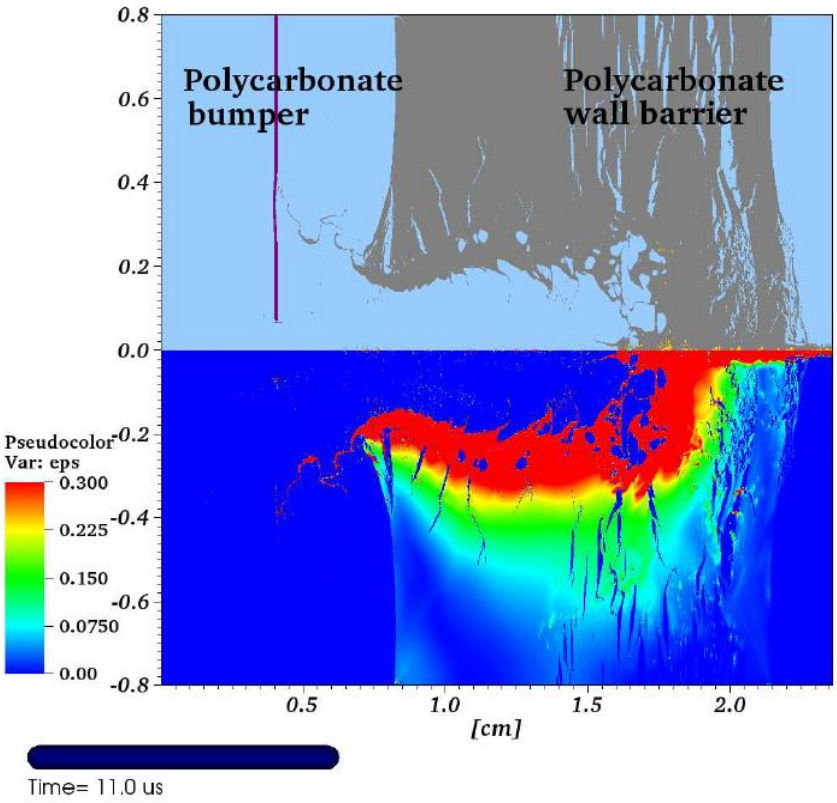

Figure 13. End state of polycarbonate wall after arresting debris

4.3 Post-shot cover

After the shot, disturbances of contaminated surfaces will be controlled with the installation of a nylon cover, as shown in Figure 14. The nose cone will be covered before proceeding to other post-shot diagnostic operations, such as image plate retrieval. The covered assembly will be removed as a single unit and transported for target material assay.

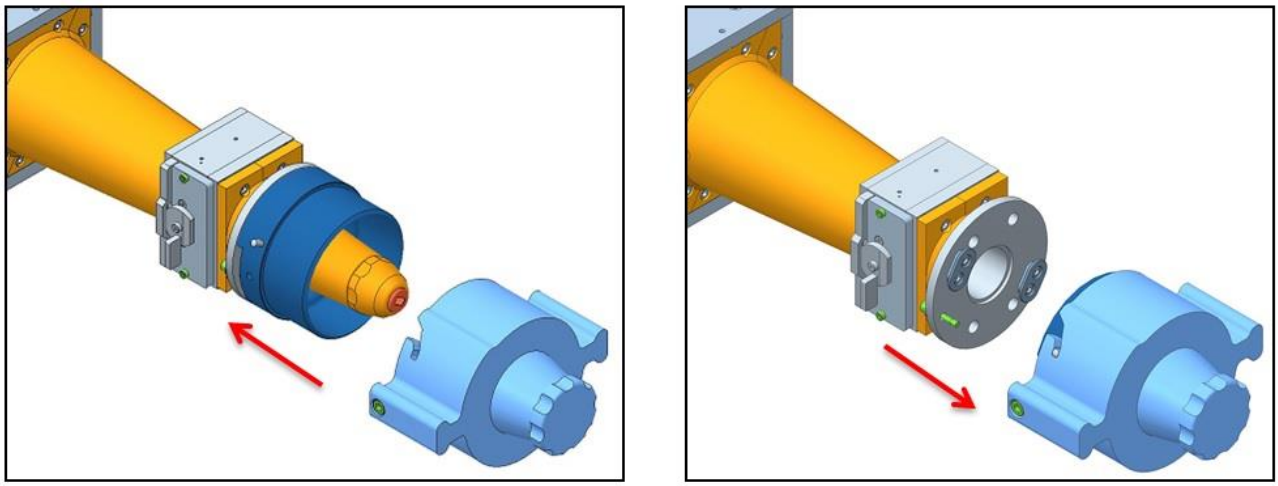

Figure 14. The HEIDI-C post-shot cover minimizes disturbances of the contaminated nose cone during operations.

5. TEST SHOTS

Two test shots were conducted using a 25 µm thick aluminum bumper and a 2.5 mm thick polycarbonate wall. These thicknesses were determined based on physics requirements and are thinner than the recommended barrier thickness based on the debris and shrapnel analysis. These test shots did not include the new external shielding. For both shots, the bumper was destroyed, as expected. The wall incurred damage, but remained intact, without penetrations. Figure 15 shows one wall after use. The wall remained intact, however some material escaped around the edges. To mitigate this, sealant will be added to the polycarbonate-nose cone interface.

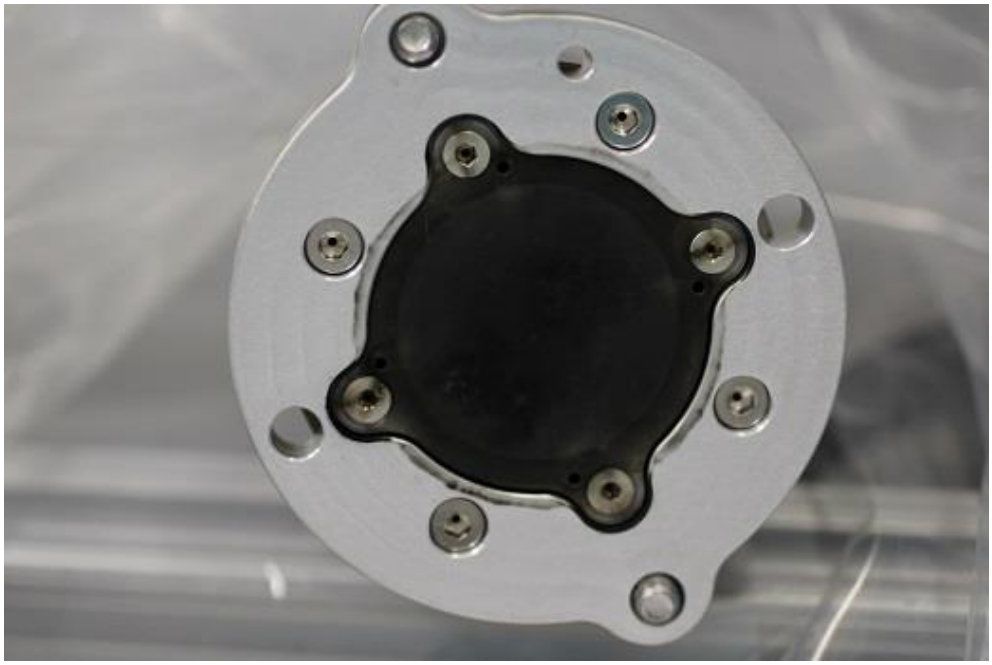

Figure 15. Post-shot image of rear wall. Wall was not penetrated, however some material escaped around wall edges.

5.1 Activated Catcher Experiment (ACE)

One of the two test shots was part of a series of experiments called the Activated Catcher Experiment (ACE). The ACE shots include various activated tracer materials in the experimental package. The components were sent for material assay, to measure the locations and amounts of the material of interest that was collected. The nose cone assembly was assayed in three separate sections, with the cap removed and assayed separately. The top portion of the nosecone indicates the side closest to the target and includes the aperture. Approximately 60% of the material of interest was recovered. Table 1 shows the location of the assayed material.

Table 1. Location of assayed target material from ACE experiment.

Component (report designation)	**% of material of interest recovered**
Debris shields (original unmodified design)	0.8
Filter materials	0.75
Nose cone assembly (bottom ≈ 1cm)	28
Nose cone assembly (top ≈ 2cm)	0
Nose cone assembly (remaining)	28
Snout cap and aperture	1.4
Total material of interest recovered	**58.95**

6. CONCLUSIONS

HEIDI has been deployed during five experimental shots. In the five experiments, none of the large, damaging debris has entered HEIDI's snout. However, large debris has been found on the nose cap near the edge of the aperture, so it must be concluded that it is possible for this debris to enter the snout. The recommended barrier thickness must be balanced with the physics requirements, which may limit the acceptable attenuation of the x-ray signal. In the event that internal shielding is penetrated, operational controls minimize the risk of spreading contamination in the facility.

Additional ACE tests will be performed with the upgraded external shielding, thickened internal shielding, and the addition of an epoxy sealant to the interfaces where target material leakage has been found. These tests will continue to assess the physical damage to the diagnostic caused by debris and the quality of the x-ray images. Further material assay measurements will help to understand the predictability of the amount of material of interest that can be collected, and to provide a quantitative analysis as part of the LLNL implementation of the ALARA principles.

This work was performed under the auspices of the U.S. Department of Energy by Lawrence Livermore National Laboratory under Contract DE-AC52-07NA27344.

REFERENCES

[1] E. I. Moses, R. N. Boyd, B. A. Remington, C. J. Keane, and R. Al-Ayat, "The National Ignition Facility: Ushering in a new age for high energy density science," AIP Physics of Plasmas 16, 041006 (2009)

[2] J.H. Hammer, "HED Experiments on NIF", 40th IEEE International Conference on Plasma Science (ICOPS), 2013

[3] W. Hsing, "Delivering High Energy Density Physics Data on the National Ignition Facility to Validate Predictive Physics Models, Hsing", Lawrence Livermore National Laboratory document, LLNL-AR-447556, 2010

[4] G. Gallegos, "Environmental ALARA Program Plan, Gretchen Gallegos", LLNL Technical Report, UCRL-AR-138061-REV-3, 2014

[5] "Diagnostic Instrument Manipulator (DIM) upgrades for reliability and operational efficiency in a radiological contamination environment at the National Ignition Facility (NIF)", Proceedings of SPIE Vol. 8850, 885005, 2013

[6] B. R. Maddox, H.-S. Park, B. A. Remington, N. Izumi, S. Chen, C. Chen, G. Kimminau, Z. A. Ali, M. J. Haugh, Q. Ma, "Characterization of the FLA7000 Image Plate System for Quantitative X-ray Detection Applications," AIP Review of Scientific Instruments, 2009

[7] A. L. Nichols "ALE3D: An Arbitrary Lagrange/Eulerian 2D and 3D Code System," Version 4.16, LLNL Technical Report, LLNL-SM-531811, Jan. 31, 2012.